Collective rotation of an oblate nucleus at very high spin

C. M. Petrache,[1] S. Frauendorf,[2] B. F. Lv,[1] A. Astier,[1] E. Dupont,[1] S. Guo,[3] M. L. Liu,[3] X. H. Zhou,[3] K. L. Wang,[3]
P. T. Greenlees,[4] H. Badran,[4] D. M. Cox,[4,*] T. Grahn,[4] R. Julin,[4] S. Juutinen,[4] J. Konki,[4,†] J. Pakarinen,[4] P. Papadakis,[4,‡]
J. Partanen,[4] P. Rahkila,[4] M. Sandzelius,[4] J. Saren,[4] C. Scholey,[4] J. Sorri,[4,§] S. Stolze,[4,‖] J. Uusitalo,[4] B. Cederwall,[5]
Ö. Aktas,[5] A. Ertoprak,[5] H. Liu,[5] I. Kuti,[6] J. Timár,[6] A. Tucholski,[7] J. Srebrny,[7] and C. Andreoiu[8]

[1]*Centre de Sciences Nucléaires et Sciences de la Matière, CNRS/IN2P3, Université Paris-Saclay, Bâtiment 104-108, 91405 Orsay, France*
[2]*Department of Physics, University of Notre Dame, Indiana 46557, USA*
[3]*Institute of Modern Physics, Chinese Academy of Sciences, Lanzhou 730000, China*
[4]*Department of Physics, University of Jyväskylä, P.O. Box 35, FI-40014 University of Jyväskylä, Finland*
[5]*KTH Department of Physics, S-10691 Stockholm, Sweden*
[6]*Institute of Nuclear Research, Hungarian Academy of Sciences, 4001 Debrecen, Hungary*
[7]*University of Warsaw, Heavy Ion Laboratory, Pasteura 5a, 02-093 Warsaw, Poland*
[8]*Department of Chemistry, Simon Fraser University, Burnaby, British Columbia V5A 1S6, Canada*

A sequence of nine almost equidistant quadrupole transitions is observed in ^{137}Nd. The sequence represents an extremely regular rotational band that extends to a spin of about 75/2 and an excitation energy of ≈ 4.5 MeV above yrast. Cranked mean-field calculations of the Nilsson-Strutinsky type suggest an oblate shape for the band. They reproduce the observed $I(I+1)$ dependence of the rotational energy whereas predicting a pronounced decrease in the deformation, which is the hallmark of antimagnetic rotation.

The dominance of prolate nuclear ground-state shapes for medium- and heavy-mass nuclei (see, e.g., Ref. [1]) is a shell effect that is caused by the thin surface layer of the nuclear potential (see, e.g., Ref. [2] and references therein). Prolate nuclei rotate collectively about the short axis. Bands representing collective rotation about the long axis of the oblate shape are exceptions, which seem to appear mainly in coexistence with prolate bands. One example is the proton-rich Pb nuclei for which the coexistence of prolate, oblate, and spherical shapes were predicted in Ref. [3] and experimentally verified in Ref. [4–7]. The interplay between rotational energy and valence orbital occupation decides the competition between oblate and prolate shapes. This was demonstrated for the proton-rich Hg isotopes in Ref. [8] and the region around ^{74}Kr in Ref. [9]. These early studies initiated extended subsequent work on shape existence, which was reviewed in Refs. [10–13]. For moderate high spins, even-spin bands were interpreted as collective rotation based on oblate shapes coexisting with prolate rotational bands in ^{186}Pb [6,7] and ^{180}Hf [14]. Oblate shapes also appear in terminating bands

[15]. Via a sequence of triaxial shapes, the bands terminate at oblate shapes where the angular momentum is the sum of the spins of the valence particles, which are aligned with the short axis as permitted by the Pauli principle. At high spins, prolate superdeformed bands cross the yrast line [16], which reflect the tendency for elongated shapes on the path toward fission instability at the critical angular momentum. To our knowledge, there is no evidence for coexisting oblate shapes at very high spins.

The present Rapid Communication reports for the first time an extremely regular rotational band developed to very high spins in the nucleus ^{137}Nd. We propose an interpretation in terms of rotation of an oblate nucleus with antimagnetic configuration. The reported results were obtained in a high-statistics spectroscopic study of Nd nuclei using the ^{100}Mo(^{40}Ar, xn) reaction with a 152-MeV ^{40}Ar beam provided by the K130 Cyclotron at the University of Jyväskylä, Finland and a self-supporting enriched ^{100}Mo foil of 0.50-mg/cm^2 thickness. A number of 5.1×10^{10} three-fold and higher prompt γ-ray coincidence events were accumulated using the JUROGAM II array. The events were time stamped by the total data readout data acquisition [17] and sorted using the GRAIN code [18]. Fully symmetrized three-dimensional (E_γ-E_γ-E_γ) and four-dimensional (E_γ-E_γ-E_γ-E_γ) matrices were analyzed using the RADWARE [19,20] analysis package. Details of the experiment and the data analysis can be found in a forthcoming paper on ^{136}Nd [21].

Figure 1 shows a partial level scheme of ^{137}Nd with the newly observed band O (to indicate the suggested interpretation as oblate band) and its tentative placement in the level
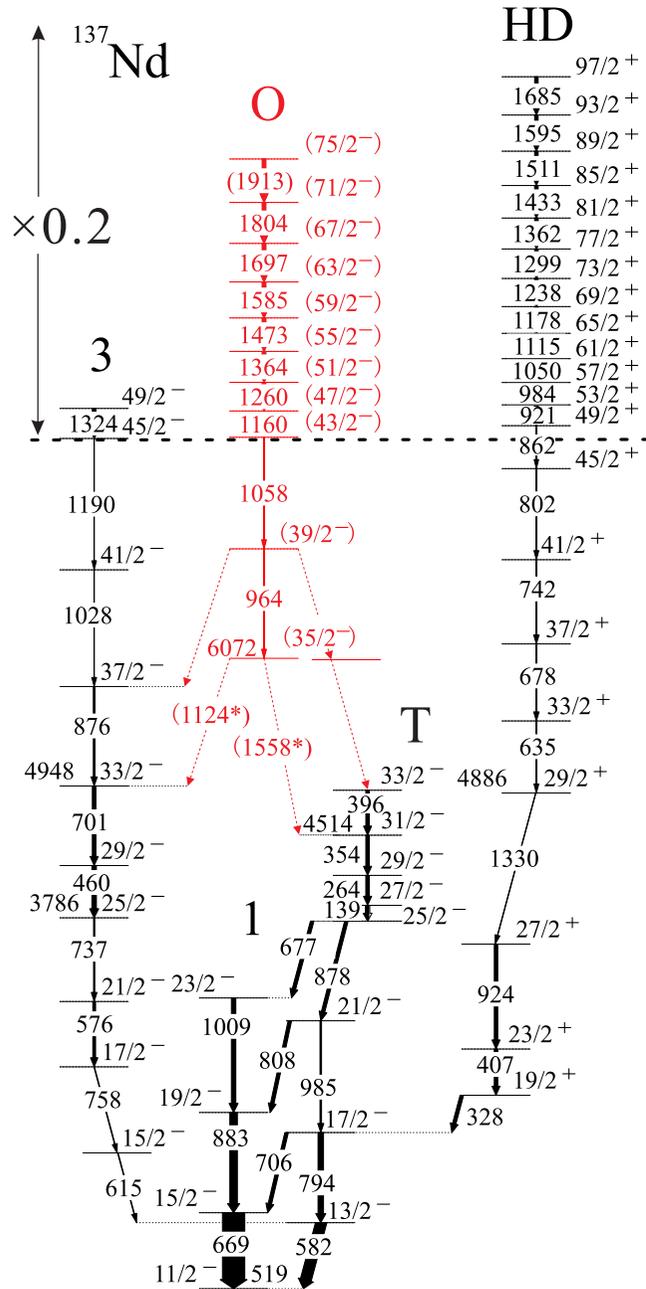
FIG. 1. Partial level scheme of ^{137}Nd showing the newly identified band O and its decay out. Possible decay-out transitions drawn with dashed lines are marked by an asterisk.

FIG. 2. Spectrum constructed by double-gating on the observed transitions of band O of ^{137}Nd. The in-band transitions are marked with red labels, whereas the low-lying transition are marked in black. Possible decay-out transitions are marked by an asterisk. The levels deexcited by the 328-, 407-, and 876-keV transitions are fed by pathways which can be found in Ref. [22].

are observed. As seen in Figs. 1 and 2, band O feeds states of bands 3 and T above the $33/2^-$ and $31/2^-$ states, respectively. The 460- and 701-keV transitions of band 3 and the 139-, 264-, and 354-keV transitions of band T are dominating the double-gated spectrum of Fig. 2 and are present in all spectra double-gated on pairs of in-band transitions of band O as well as in spectra double-gated on in-band transitions and transitions of bands 3 or T. The intensity of the 964-keV transition is lower than the one of the 1058-keV transition. Taking into account the systematic increase in the intensity with decreasing transition energy, it means that there must be substantial decay out from the level deexcited by the 964-keV in-band transition. The two feeble peaks at 1124 and 1558 keV might be transitions out of the lowest level of band O as suggested by the dotted lines in Fig. 1. However, they are too weak to account for the entire intensity of band O. In addition, the 876- and 396-keV transitions of bands 3 and T [22], which populate the $33/2^-$ and $31/2^-$ of bands 3 and T, respectively, are present in some double-gated spectra, indicating weak decay-out pathways of band O towards the $37/2^-$ and $33/2^-$ states of bands 3 and T, respectively, and strongly suggesting that the band-head spin is smaller than $39/2$.

The tentative lines connecting band O with the $33/2^-$ state of band 3 and the $31/2^-$ state of band T suggest a spin-parity $35/2^-$ of the bandhead and $M1$ and $E2$ characters for the respective transitions. A less plausible alternative spin assignment is $33/2$. The absence of any transitions above the 876-keV transition of band 3 and above the 396-keV transition of band T indicates that the spin of the bandhead of band O must be smaller than $39/2$. In any case, a bandhead spin lower by one unit would make band O even more nonyrast. On the other hand, a bandhead spin higher than $35/2$ by $1\hbar$ or $2\hbar$ will make band O more yrast, which is in contrast with its very weak intensity of $\approx 1\%$ and anyway will not change the conclusions of the present Rapid Communication because the band would remain very nonyrast at the highest spins (≈ 4.1 or ≈ 3.7 MeV for bandhead spin 37/3 or 39/2, respectively). The present experimental information

scheme, together with the highly deformed (HD) band and bands 1, 3, and 6 observed in Ref. [22] (band 6 is labeled T in the present Rapid Communication to indicate the suggested interpretation as triaxial band). A double-gated spectrum of band O is given in Fig. 2. The spectrum is obtained from the E_γ-E_γ-E_γ cube by gating on two axes on each couple of different in-band transitions and projecting on the third axis the sum of all double-gated resulting spectra.

The intensity of band O is smaller than 1% of the total population of the nucleus. The decay-out must be fractionated among several transitions because no strong decay-out lines
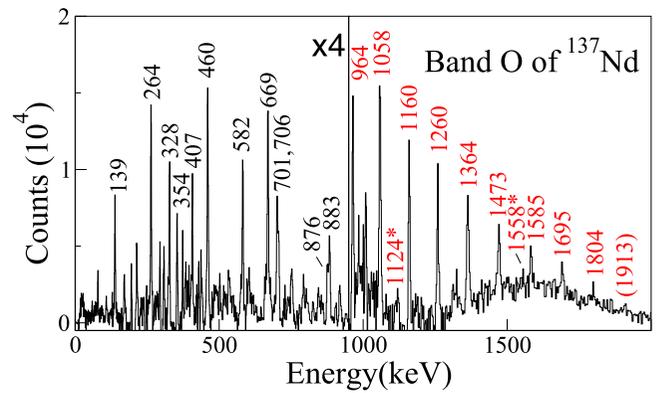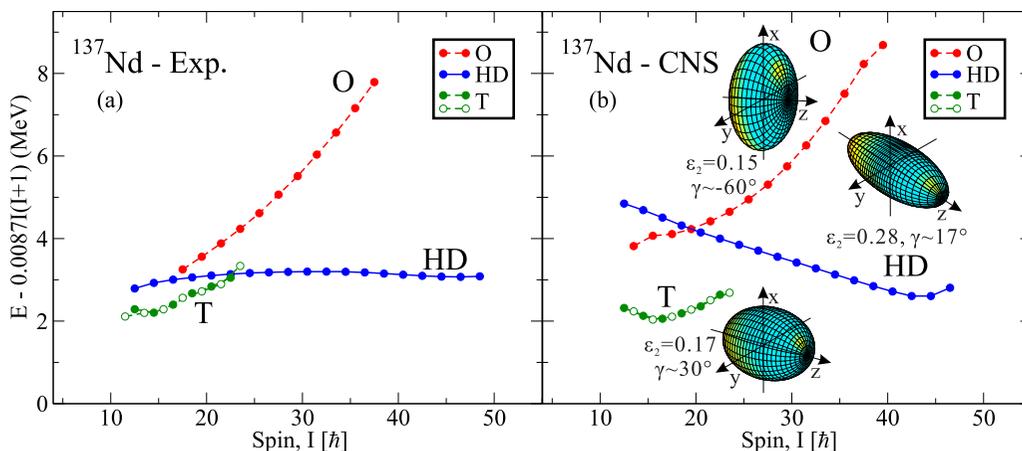
FIG. 3. (a) Experimental energies relative to a rigid body rotor for the bands O, HD, and T of ^{137}Nd. (b) Energies relative to a rotating liquid drop calculated by means of the cranked Nilsson-Strutinsky (CNS) approach for the bands O, HD, and T. Open and filled symbols used for band T correspond to the two signature partners of the dipole band.

provides convincing evidence for the existence of a rotational $\Delta I = 2$ sequence that starts between $I = 33/2$ and $39/2$, and excitation energy between 6 and 7 MeV. For the following discussion, we assume the most likely assignment of $35/2^-$ to the bandhead of band O, which is displayed in Fig. 1. As discussed below, this assignment is strongly supported by the theoretical interpretation.

Figure 3(a) shows the energies of the new band together with energies of selected bands that were known before [22]. As observed in Ref. [22], the HD band becomes yrast above spin $20\hbar$. The new band O has a moment of inertia that is only $2/3$ of the one of the HD band [the slopes of the functions $I(\omega)$ in Fig. 4]. As a consequence, it moves rapidly away from the yrast line [see Fig. 3(b)].

In order to find out the structure of band O we carried out calculations in the framework of the CNS mean-field approach [15,23]. In the CNS formalism, the nucleus rotates about
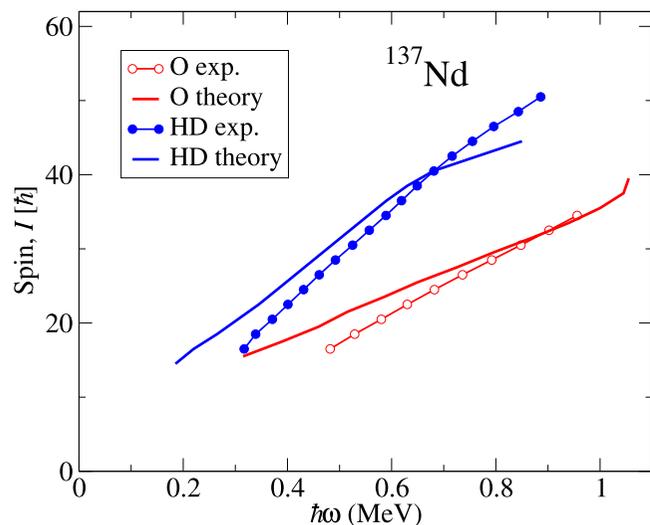
one of the principal axes of the triaxial modified harmonic-oscillator (Nilsson) potential (parameters cf. Refs. [15,23]), and pairing correlations are neglected.

The total energy $E(I, \varepsilon, \gamma)$ of a given single-particle configuration is calculated as a function of the deformation parameters (ε, γ) and the equilibrium found as the minimum. Figure 5 shows such surfaces for the considered bands. We use the Lund convention for the triaxiality parameter γ. The prolate shape corresponds to $\gamma = 0°, -120°$, and the oblate

FIG. 4. Angular momentum as a function of the rotational frequency $\hbar\omega = [E(I) - E(I-2)]/2$ of bands O and HD.
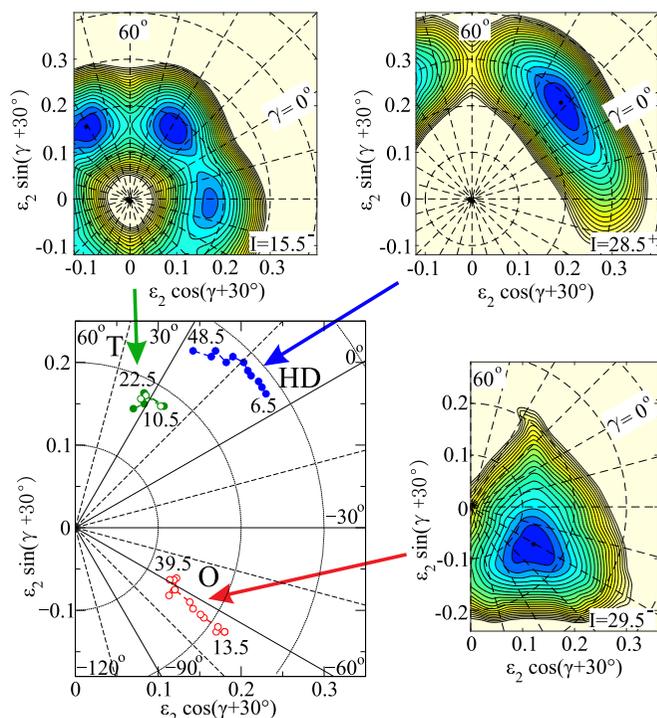

FIG. 5. Deformation trajectories as a function of spin and potential-energy surfaces for the bands O, HD, and T of ^{137}Nd. Open and filled symbols correspond to $\alpha = -1/2$ and $\alpha = +1/2$, respectively. The distance between the contour lines is 0.25 MeV.
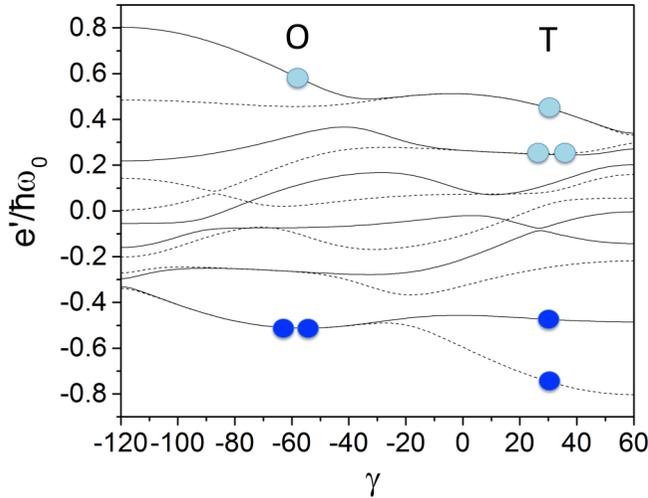
FIG. 6. Single-particle Routhians of the $h_{11/2}$ shell as a function of the triaxiality parameter γ for the j-shell model of Ref. [24]. The shown case corresponds to the bottom of band O and the middle of band T. The rotational frequency is $\hbar\omega = 0.45$ MeV, and the energy scale is $\hbar\omega_0 = 8$ MeV. Full line: favored signature; dashed line: unfavored signature ($-1/2$ and $1/2$, respectively, for $h_{11/2}$), blue circles: protons; cyan circles: neutron holes.
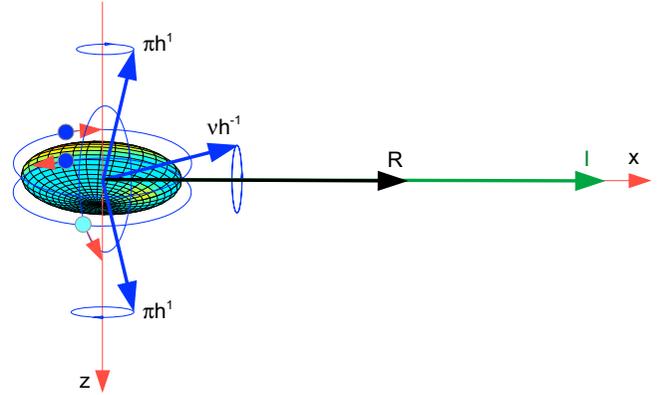

FIG. 7. Angular momentum composition of band O. The $h_{11/2}$ orbitals are represented by their individual j vectors. The sum of the contributions of the normal-parity orbitals, which are not shown in the figure, is denoted by R. The total angular momentum I is the sum of the projections on the rotational (x) axis.

shape corresponds to $\gamma = \pm 60°$. The values $\pm\gamma, 120° - \gamma$ correspond to the same triaxial shape where the rotation (x) axis is the shortest principal axis for $0 < \gamma < 60°$, the intermediate principal axis for $-60° < \gamma < 0$, and the long principal axis for $-120° < \gamma < -60$. The various bands are characterized by their parity π, signature $\alpha = I + 2n$, n even, and the occupation of the high-j orbitals $h_{11/2}, i_{13/2}$.

Only the region $I > 13$ is considered for band O because below pairing correlations become important. We found three types of states, which are represented by the three examples in Figs. 3(b) and 5. The group of triaxial bands has a deformation of $(\varepsilon_2, \gamma) \approx (0.17, 20°)$. We show band 6 of Ref. [22] as an example [labeled by T in Figs. 3(b), 4, and 6] to which we assign the configuration $[\pi h_{11/2}^2 \times \nu h_{11/2}^{-3}]$. The physics of related $\Delta I = 1$ bands in ^{135,136,138}Nd has been discussed in Refs. [25–27]. The group of highly deformed bands has $(\varepsilon_2, \gamma) \approx (0.28, +15°)$. The lowest is the yrast band HD with the configuration $[\pi h_{11/2}^4 \times \nu h_{11/2}^{-4} h_{9/2}^2 i_{13/2}]$. The short principal axis is the rotational axis. The third group consists of bands with near-oblate shapes $(\varepsilon_2, \gamma) \approx (0.15, -60°)$ with the rotational axis perpendicular to the symmetry axis. The lowest configuration is $[\pi h_{11/2}^2 \times \nu h_{11/2}^{-1}]$ with $(\pi, \alpha) = (-, 1/2)$ (see Fig. 6). Its angular momentum geometry is illustrated in Fig. 7. We associate it with band O assuming the spin-parity assignment suggested in Fig. 1. As seen in Figs. 3 and 4, the CNS calculations well reproduce the experiment.

Frauendorf [24] analyzed in detail the interplay between high-j particles and the deformed potential in the framework of a j-shell model. Figure 6 shows the single-particle Routhians for a frequency that corresponds to the low part of band O and the middle part of band T. For $\gamma \approx 30°$, the two degenerate signatures of the $\nu h_{11/2}$ hole generate a $\Delta I = 1$ band, which is the characteristic of band T. For $\gamma \approx -60°$, the

lowest $\nu h_{11/2}$ hole has $\alpha = +1/2$ and is well separated from the next hole state with $\alpha = -1/2$. That is, the observation of only one $\Delta I = 2$ sequence supports the assignment of the oblate shape. The large signature splitting supports our tentative spin assignment. If the hole state had the unfavored signature, the question arises, why the lower band with the favored signature is not observed?

As seen in Fig. 6, the two $h_{11/2}$ protons (blue circles) drive toward oblate shape with a preference of $\gamma = 60°$ for a finite rotational frequency. The odd $h_{11/2}$ neutron hole drives toward prolate shape with a preference of $\gamma = -120°$ for finite rotational frequency. The polarization trends reflect maximization of the overlap of the particle orbitals and minimization of the hole orbitals with the deformed potential and the "deformation-assisted rotational alignment" discussed in Ref. [24]. In case of band T, the two opposite trends balance at $\gamma \approx 30°$. For band O, the balance is shifted to $\gamma \approx -60°$ because two neutron holes are excited to the (dg) orbitals. They increase the collective rotational energy of the core, which has the irrotational-flow γ dependence $\propto [\sin(\gamma - 60°)]^{-2}$ driving toward the negative γ side.

Band O follows closely the rigid rotor rule $I(I + 1)/2\mathcal{J}_O$ with $\mathcal{J}_O \approx 39$ $\hbar^2$ MeV^{-1}, whereas the deformation continuously decreases (cf. Fig. 5). This is characteristic for antimagnetic rotation (see Ref. [28]). At the bottom of the band, the two $h_{11/2}$ proton orbitals are back to back and perpendicular to the symmetry axis as shown in Fig. 7. Along the band, their j vectors gradually align with the rotational x axis increasing the total angular momentum I. A simple model assuming linear polarization of the core composed of the low-spin nucleons by the high-j nucleons accounts for the $E \propto I(I + 1)$ dependence and the simultaneous decrease in the deformation [28]. Our CNS calculations predict the $B(E2)$ values change gradually along band O, being 0.58, 0.54, 0.46, 0.43, 0.37, 0.31, 0.26, 0.28, 0.19, and 0.23 e^2b^2 for in-band transitions from the levels with $I = 39/2, 43/2, 47/2, 51/2, 55/2, 59/2, 63/2, 67/2, 71/2, 75/2$, respectively.

As can be deduced from Fig. 4, the CNS calculations underestimate the kinematic moment of inertia (slope) by about 25% and give a constant amount of aligned angular momentum (intercept with the y axis) of about $10\hbar$, that is not seen in the experiment. The discrepancy might indicate the presence of residual pair correlations that are gradually quenched by rotation.

To summarize, an extremely regular rotational band in ^{137}Nd has been observed, which extends to a tentative spin of $I = 75/2$. As its average moment of inertia of $39.3\hbar^2$ MeV^{-1} is only 2/3 of the moment of inertia of $56.9\hbar^2$ MeV^{-1} of the highly deformed yrast band, it reaches an excitation energy of ≈ 4.5 MeV above the yrast line. The existence of an individual collective rotational band in the environment of the dense background of damped bands at such high excitation energy is a surprising observation. It signals a drastic structural difference from its environment. Calculations in the framework of the CNS version suggest for the new band a moderately deformed oblate shape rotating about the long axis and for the damped background bands a strongly deformed prolate shape rotating about the short axis. A theoretical investigation if this difference in shape ensures the existence of the new band is on the way but beyond the present article. The CNS calculations reproduce rather well the observed $\propto I(I + 1)$ rotational energy while predicting a pronounced decrease in deformation, which is the hallmark of antimagnetic rotation. The band is the longest antimagnetic rotational sequence observed so far. Measuring the lifetimes of the transitions would be important to confirm the predicted decrease in deformation and thus support the suggested interpretation.

[1] Z. Podolyák, J. Phys.: Conf. Ser. **381**, 012052 (2012).

[2] S. Frauendorf and C. Guet, Annu. Rev. Nucl. Part. Sci. **51**, 219 (2001).

[3] F. R. May, V. V. Pashkevich, and S. Frauendorf, Phys. Lett. B **68**, 113 (1977).

[4] J. Heese *et al.*, Phys. Lett. B **302**, 390 (1993).

[5] A. M. Baxter *et al.*, Phys. Rev. C **48**, R2140(R) (1993).

[6] J. Pakarinen *et al.*, Phys. Rev. C **72**, 011304(R) (2005).

[7] J. Pakarinen *et al.*, Phys. Rev. C **75**, 014302 (2007).

[8] S. Frauendorf and V. V. Pashkevich, Phys. Lett. B **55**, 365 (1975).

[9] J. H. Hamilton *et al.*, J. Phys. G.: Nucl. Part. Phys. **10**, L87 (1984).

[10] K. Heyde, P. V. Isacker, M. Waroquier, J. L. Wood, and R. A. Meyer, Phys. Rep. **102**, 291 (1983).

[11] J. L. Wood, K. Heyde, W. Nazarewicz, M. Huyse, and P. V. Duppen, Phys. Rep. **215**, 101 (1992).

[12] K. Heyde and J. L. Wood, Rev. Mod. Phys. **83**, 1467 (2011).

[13] R. Julin, T. Grahn, J. Pakarinen, and P. Rahkila, J. Phys. G.: Nucl. Part. Phys. **43**, 024004 (2016).

[14] U. S. Tandel *et al.*, Phys. Rev. Lett. **101**, 182503 (2008).

[15] A. V. Afanasjev, D. B. Fossan, G. J. Lane, and I. Ragnarsson, Phys. Rep. **322**, 1 (1999).

[16] B. Singh, R. Zywina, and R. B.Firestone, Nucl. Data Sheets **97**, 241 (2002).

[17] I. H. Lazarus *et al.*, IEEE Trans. Nucl. Sci. **48**, 567 (2001).

[18] P. Rahkila, Nucl. Instrum. Methods Phys. Res., Sect. A **595**, 637 (2008).

[19] D. Radford, Nucl. Instrum. Methods Phys. Res., Sect. A **361**, 297 (1995).

[20] D. Radford, Nucl. Instrum. Methods Phys. Res. Sect. A **361**, 306 (1995).

[21] B. F. Lv *et al.*, Phys. Rev. C **98**, 044304 (2018).

[22] C. M. Petrache *et al.*, Nucl. Phys. A **617**, 228 (1997).

[23] T. Bengtsson and I. Ragnarsson, Nucl. Phys. A **436**, 14 (1985).

[24] S. Frauendorf, Phys. Scr. **93**, 043003 (2018).

[25] S. Mukhopadhyay *et al.*, Phys. Rev. Lett. **99**, 172501 (2007).

[26] S. Mukhopadhyay *et al.*, Phys. Rev. C **78**, 034311 (2008).

[27] C. M. Petrache *et al.*, Phys. Rev. C **86**, 044321 (2012).

[28] S. Frauendorf, Rev. Mod. Phys. **73**, 463 (2001).